

Theory of diffraction for 2D photonic crystals with a boundary

D. Felbacq, E. Centeno
LASMEA UMR-CNRS 6602
Complexe des Cézeaux
63177 Aubière Cedex
France

Abstract

We extend a modal theory of diffraction by a set of parallel fibers to deal with the case of a hard boundary: that is a structure made for instance of air-holes inside a dielectric matrix. Numerical examples are given concerning some resonant phenomena.

I. INTRODUCTION

Photonic crystals (PCs) are periodically modulated structures that present the properties of having photonic band gaps [1–3]. In the case of 2D photonic crystal where it is possible to study separately *s*- and *p*-polarized fields, it is now known that large gaps are easier to obtain with inverted-contrast crystals (i.e. air holes in a dielectric matrix) with *p*-polarized fields than with *s*-polarized fields [4,5]. In this work we extend a multi-scattering theory by cylinders [4,6–9] in order to deal with inverted-contrast crystals with a hard boundary, that is a structure made of dielectric or metallic inclusions in a dielectric matrix embedded in vacuum (fig. 1). This theory allows to quantify the importance of the hard boundary when the device is considered as a 2D PC and also to study the propagation phenomena when the device modelizes a photonic crystal fiber [10–13].

II. THEORY OF DIFFRACTION

We start by constructing the generalized scattering matrix of a set of N dielectric or metallic rods embedded in a dielectric cylinder of circular cross section Ω (fig.1) and radius R . We use a Cartesian coordinate system $(O; x, y, z)$ with origin at the center of Ω . The electromagnetic fields considered here are harmonic fields with a time dependence of $\exp(-i\omega t)$.

The rods are denoted by $\{D_n\}$, they are filled with a dielectric (relative permittivity ε_n) or metallic material. The cylinder in which the fibers are contained has relative permittivity ε_r , finally this cylinder is embedded in vacuum. Due to the invariance of the medium along the z -direction we look for solutions of Maxwell equations with a z dependence of $\exp(i\gamma z)$. Under this assumption, it is easily shown that all the components of both magnetic and electric fields are known once E_z and H_z are known. Denoting

$$\mathbf{F} = \begin{pmatrix} E_z \\ H_z \end{pmatrix},$$

the following propagation equation is satisfied

$$\Delta_{\perp} \mathbf{F} + \chi^2 \mathbf{F} = 0$$

we denote $\Delta_{\perp} = \frac{\partial^2}{\partial x^2} + \frac{\partial^2}{\partial y^2}$, $\chi^2 = k^2 \varepsilon(x) - \gamma^2$ and k is the wavenumber. We denote

$$\begin{cases} \chi_r^2 = k^2 \varepsilon_r - \gamma^2 \\ \chi_n^2 = k^2 \varepsilon_n - \gamma^2 \\ \chi_0^2 = k^2 \varepsilon_0 - \gamma^2 \end{cases}$$

The total exterior field \mathbf{F} is expanded in Fourier-Bessel expansion outside Ω

$$\mathbf{F}(r, \varphi) = \sum_m [\mathbf{F}_m^{i,+} J_m(\chi_0 r) + \mathbf{F}_m^{d,+} H_m^{(1)}(\chi_0 r)] e^{im\varphi}, \quad |r| \geq R \quad (1)$$

Remark: $\sum_m \mathbf{F}_m^{i,+} J_m(\chi_0 r) e^{im\varphi}$ represents the incident field.

The total field \mathbf{F} inside Ω writes in the vicinity of the boundary $\partial\Omega$ of Ω

$$\mathbf{F}(r, \varphi) = \sum_m [\mathbf{F}_m^{i,-} J_m(\chi_r r) + \mathbf{F}_m^{d,-} H_m^{(1)}(\chi_r r)] e^{im\varphi} \quad (2)$$

We denote

$$\widehat{\mathbf{F}}^{i,\pm} = (\mathbf{F}_m^{i,\pm})_{m \in \mathbb{Z}}, \quad \widehat{\mathbf{F}}^{d,\pm} = (\mathbf{F}_m^{d,\pm})_{m \in \mathbb{Z}}$$

so that the transmission conditions on $\partial\Omega$ write

$$\begin{aligned} \widehat{\mathbf{F}}^{i,+} + \widehat{\mathbf{F}}^{d,+} &= \widehat{\mathbf{F}}^{i,-} + \widehat{\mathbf{F}}^{d,-} \\ \mathbf{L}_{\varphi}^+ [\widehat{\mathbf{F}}^{i,+} + \widehat{\mathbf{F}}^{d,+}] &= \mathbf{L}_{\varphi}^- [\widehat{\mathbf{F}}^{d,+} + \widehat{\mathbf{F}}^{d,-}] \end{aligned} \quad (3)$$

where $\mathbf{L}_{\varphi}^{\pm}$ are boundary impedance operators easily deduced from Maxwell equations. Conditions (3) lead to

$$\begin{pmatrix} \widehat{\mathbf{F}}^{i,-} \\ \widehat{\mathbf{F}}^{d,+} \end{pmatrix} = \begin{bmatrix} \mathcal{S}_1^- & \mathcal{S}_2^- \\ \mathcal{S}_1^+ & \mathcal{S}_2^+ \end{bmatrix} \begin{pmatrix} \widehat{\mathbf{F}}^{i,+} \\ \widehat{\mathbf{F}}^{d,-} \end{pmatrix} \quad (4)$$

where $\mathcal{S}_{1,2}^{\pm}$ are linear operators deduced from (3) linking the incoming and outgoing parts of the fields on the boundary of Ω .

Remark: In case where the boundary is not circular the theory can still be applied provided the expansions (1-2) are restricted respectively to the smallest circle of center O containing Ω and to the greatest circle contained in Ω . In that case operators $\mathcal{S}_{1,2}^{\pm}$ have to be computed numerically (for instance using the Method of Fictitious Sources [15] or the Differential Method [16]).

Around each rod D_n the diffracted part of the field has the following expansion: $\sum_k \mathbf{F}_{n,k}^{d,-} H_k^{(1)}(\chi r_n) e^{ik\varphi_n}$ where (r_n, φ_n) are the polar coordinates associated to fiber n . The Hankel part of the total field is the sum of the fields diffracted by each rod D_n inside Ω :

$$\sum_m \mathbf{F}_m^{d,-} H_m^{(1)}(\chi r) e^{im\varphi} = \sum_{n=1}^N \sum_l \mathbf{F}_{n,l}^d H_l^{(1)}(\chi r_n) e^{il\varphi_n} \quad (5)$$

so that there is a linear operator $\mathcal{L} = (\mathcal{L}_m^n)_{m \in \mathbb{Z}}^{n=1..N}$ such that $\mathbf{F}_m^{d,-} = \sum_{n=1}^N \mathcal{L}_m^n [\hat{\mathbf{F}}_n^d]$ where $\hat{\mathbf{F}}_n^d = (\mathbf{F}_{n,l}^d)_{l \in \mathbb{Z}}$

Conversely, there is a linear operator $\mathcal{R} = (\mathcal{R}_n^m)_{n=1..N}^{m \in \mathbb{Z}}$, obtained from the translation formula for Bessel functions [17], such that $\mathcal{R}_n^l (\hat{\mathbf{F}}^{i,-}) = \mathbf{F}_{l,n}^{i,-}$. Operator \mathcal{R} is injective, i.e. it is left invertible, whereas \mathcal{L} is surjective, i.e. it is right invertible: $\mathcal{L} \times \mathcal{R} = N \mathbb{I}_d$. The multi-scattering theory without boundary [4,6–9] shows that it is possible to define a linear operator \mathcal{H} such that

$$\mathcal{H}^{-1} \begin{pmatrix} \hat{\mathbf{F}}_1^d \\ \vdots \\ \hat{\mathbf{F}}_N^d \end{pmatrix} = \mathcal{R} \hat{\mathbf{F}}^{i,-} \quad (6)$$

from which we derive the scattering matrix of the system of rods in the absence of a boundary, that is when the medium of permittivity ε_r fills the entire space: $\mathcal{S}_{wb} = \mathcal{L} \mathcal{H} \mathcal{R}$, which satisfies $\hat{\mathbf{F}}^{d,-} = \mathcal{S}_{wb} \hat{\mathbf{F}}^{i,-}$. System (4) then rewrites

$$\begin{pmatrix} \hat{\mathbf{F}}^{i,-} \\ \hat{\mathbf{F}}^{d,+} \end{pmatrix} = \begin{bmatrix} \mathcal{S}_1^- & \mathcal{S}_2^- \mathcal{S}_{wb} \\ \mathcal{S}_1^+ & \mathcal{S}_2^+ \mathcal{S}_{wb} \end{bmatrix} \begin{pmatrix} \hat{\mathbf{F}}^{i,+} \\ \hat{\mathbf{F}}^{i,-} \end{pmatrix} \quad (7)$$

from which we derive the expression of the internal and exterior fields from the incident field:

$$\begin{cases} \hat{\mathbf{F}}^{i,-} = (I_d + \mathcal{S}_2^- \mathcal{S}_{wb})^{-1} \mathcal{S}_1^- \hat{\mathbf{F}}^{i,+} \\ \hat{\mathbf{F}}^{d,-} = \mathcal{S}_{wb} (I_d + \mathcal{S}_2^- \mathcal{S}_{wb})^{-1} \mathcal{S}_1^- \hat{\mathbf{F}}^{i,+} \\ \hat{\mathbf{F}}^{d,+} = [\mathcal{S}_1^+ + \mathcal{S}_2^+ \mathcal{S}_{wb} (I_d + \mathcal{S}_2^- \mathcal{S}_{wb})^{-1} \mathcal{S}_1^-] \hat{\mathbf{F}}^{i,+} \end{cases} \quad (8)$$

and the problem is solved. This formulation allows to use distinct numbers n_c (exterior cylinder) and n_f (fibers) of Fourier-Bessel coefficients. This point is a crucial advantage for a low computation time. Indeed, for a given wavelength the interior diffraction problem may be correctly described with a small number of Fourier-Bessel coefficients n_f whereas the exterior problem requires a larger number of coefficient n_c .

In the case of a diffraction problem, $\hat{\mathbf{F}}^{i,+}$ represents the incident field illuminating the structure such as a plane wave, a gaussian beam or a cylindrical wave. The plane wave defined by the trihedron $(\mathbf{E}^i, \mathbf{H}^i, \mathbf{k}_0)$ is spatially characterized by its Euler angles $(\varphi_0, \theta_0, \delta_0)$ where φ_0 , θ_0 and δ_0 are respectively called precession, conicity and polarization angle, see fig. 2. Therefore, the Cartesian coordinates of \mathbf{k}_0 are given by:

$$\mathbf{k}_0 = \begin{cases} k_0 \sin \theta_0 \cos \varphi_0 \\ k_0 \sin \theta_0 \sin \varphi_0 \\ k_0 \cos \theta_0 \end{cases}$$

In this formalism, the case of s (resp. p) polarization is defined by the parameters $\theta_0 = 90^\circ$ and $\delta_0 = 90^\circ$ (resp. $\delta_0 = 0^\circ$). This corresponds to the cases where the unique non zero component of the electric field (resp magnetic field) is E_z (resp. H_z).

III. NUMERICAL EXAMPLE

We consider a hexagonal photonic crystal constituted by 19 air holes embedded in a dielectric circular cylinder of optical index $\sqrt{\epsilon_r} = 4$, see fig. 3. The radii of the holes and of the cylinder core are respectively equal to $r_f = 0.8$ and $R = 10$. The two-dimensional structure is illuminated by a plane wave in p -polarization. The transmission coefficient T is defined as the flux of the Poynting vector of the total field collected on a segment situated below the cylinder sheath and normalized to the incident energy, see fig 3. The convergence of the vector multi-scattering method is studied with respect to the numbers n_f and n_c of Fourier coefficients respectively used for the series expansion of the interior (fibers) and exterior (cylinder sheath) problems. Figure 4 presents the relative error of the transmission T versus n_f and n_c for an incident plane wave with $\lambda/R = 1.70$ i.e. in the resonant domain. The vector multi-scattering method converges with a relative error less than 0.1% with $n_c > 15$ and for n_f higher than 3. However, independently of n_c , the number of Fourier coefficients n_h must be higher than 4 for a correct convergence of the diffraction problem. Therefore, in order to get a good numerical convergence in this wavelength domain, we choose $n_c = 20$ and $n_f = 4$. In that case, using a Personal Computer with a 200 MHz processor and with 64 Mo of RAM, the computation time for the transmission coefficient for a wavelength and for the structure defined in fig.3 is about 50 seconds. We have also tested our results against that obtained using the fictitious Sources Method [15,14].

We now study the scattering properties of the PC embedded inside the cylinder sheath defined in fig.3:

We start with a hexagonal PC constituted by 19 air holes embedded in an infinitely dielectric medium of optical index $\sqrt{\epsilon_r} = 4$ (i.e. without the circular boundary). The PC presents a photonic band gap for the interval of wavelengths $\lambda/R = [2.0; 2.70]$ for p -polarization, see the bold curve of figure 5. The solid curve represents the transmission T of the PC without boundary and doped by a central microcavity (the central air hole is removed) computed for p -polarization ($\theta_0 = 90^\circ$ and $\delta_0 = 0^\circ$). It appears a resonant wavelength $\lambda_r(90^\circ)/R = 2.13$ inside the photonic band gap associated with a localized mode.

Let us now compare these results with that corresponding to the structure defined in fig.3 (PC with the circular boundary):

Figure 6 gives the transmission diagram versus the wavelength for a p -polarized incident plane wave. The solid curve represents the transmission in the case where the central air hole is removed whereas the dashed curve represents the transmission for the perfect crystal (with the central hole). This structure also presents a photonic band gap for the interval $[2.15; 2.7]$ but slightly shifted toward higher wavelengths in comparison with the PC without the circular boundary. We can also remark that though the cylinder sheath is illuminated in the resonant domain, the photonic band gap phenomenon provokes the extinction of the electromagnetic modes of the exterior cylinder.

The doped PC embedded inside the cylinder sheath presents a maximum of transmission inside the photonic band gap domain for the wavelength $\lambda_r^c(90^\circ)/R = 2.20$. The map of the modulus of the magnetic field confirms that the resonant wavelength $\lambda_r^c(90^\circ)/R = 2.20$ is associated to a localized mode of the structure, see fig.7. In conclusion, **the resonant wavelengths of PCs inside an infinite dielectric medium are shifted toward higher wavelengths when PCs are embedded inside a cylinder sheath.** These results

demonstrate that rigorous numerical computations of finite-size structures are necessary to efficiently describe diffraction properties of PC fibers.

Recent studies have demonstrated that resonant wavelengths associated to localized modes strongly depend upon the propagation coefficient γ (i.e. upon the conicity angle θ_0 in the case of scattering problems) [4,20]. Numerical and theoretical experiments have shown that the dependence of the resonant wavelengths with respect of the conicity angle is given by:

$$\lambda_r(\theta_0) = \lambda_r(90^\circ) \sin \theta_0 \quad (9)$$

This behavior can be interpreted thanks to a simple model called "model of the infinitely conducting cavity" [19]. Although the localization of light inside PCs doped by microcavities is a global phenomenon due to the photonic band gap effect and the broken symmetry of the lattice, both resonant wavelengths and localized modes may be well approximated using a local representation of the electromagnetic field. Figure 5 presents the diagram of transmission in the case of the doped PC without boundary for 3 distinct conicity angles 90° , 80° , 70° and for a fixed polarization angle $\delta_0 = 0^\circ$. The resonant wavelength is shifted toward the shorter wavelengths inside the band gap when the conicity angle decreases. In table 1, both numerical computations and predicted resonant wavelengths versus the conicity angle are compared. The domain of validity of the "infinitely conducting cavity" model depends on the strength of the localization of the light with respect to the conicity angle. For example in our case, decreasing the conicity angle induced the shift of the localized modes toward the lower edge of the band gap. Therefore the localized mode is delocalized out of the microcavity hence the model of "the infinitely conducting cavity" is no more valid. This behavior explains why equation (9) must be applied for low inclinations of the wave vector with respect to the plane defined by the cross section of the fibers (i.e. for $\theta < 60^\circ$). Let us now study the optical properties of the same PC embedded inside the cylinder sheath defined in fig.3 versus the conicity angle. Figure 8 presents the diagram of transmission obtained for 3 values of the conicity angle (90° , 80° , 70°) and for a fixed polarization angle $\delta_0 = 0^\circ$. These results lead to two remarks:

- 1) When decreasing the conicity angle, a second resonant wavelength appears,
- 2) The shift of the resonant wavelength is weaker for a PC fiber than for a PC without boundary.

The apparition of the second resonant wavelength $\lambda_r^c(70^\circ)/R = 2.226$ demonstrates that the optical interactions of the PC and the cylinder sheath modify strongly the photonic band structures. Moreover, the conicity angle dependence of the resonant wavelengths diminishes when the PC is embedded inside a cylinder sheath. In that case, the model of the "infinitely conducting cavity" cannot be used to compute the shift of the resonant wavelengths for grazing incidence. This behavior may be efficiently used for controlling the detuning of the localized modes with respect to the inclination of the wave vector.

IV. CONCLUSION

We have extended the vector multi-scattering theory of diffraction by parallel cylinders to the case of a hard boundary. We have applied this theory in order to study the scattering

properties of a PC embedded inside a cylinder sheath. The numerical results have shown that PC fibers present complicated photonic band structures with additional localized modes for grazing incidence. The exterior circular boundary also attenuates the detuning of the resonant wavelengths with respect to the inclination of the wave vector (i.e. with the propagation coefficient γ). Matters related to the optical effects of the size of the PC inside the cylinder sheath will be discussed in future studies. This theory allows to study the transmission properties of 2D PC with inverted contrast but it can also be straightforwardly applied to the study of propagation phenomena in photonic crystal fibers, where the modes are linked to the resonances of the scattering matrix [18,19,21] Work is also in progress in that direction

REFERENCES

- [1] J.D. Joannopoulos, R. Meade and J.Winn, *Photonic crystals*, (Princeton U. Press, Princeton, N.J., 1995).
- [2] Benisty H, Weisbuch C, Labilloy D, et al., Appl. Surf. Sci. **164**, 205 (2000).
- [3] J. Rarity and C. Weisbuch ed., *Microcavities and Photonic Bandgaps: Physics and Applications* (NATO ASI Series, Kluwer Academic Publishers, The Netherlands, 1996).
- [4] E. Centeno, D. Felbacq, J. Opt. Soc. Am. A **17**, 320 (2000).
- [5] D. Maystre, Pure Appl. Opt, **3**, 975, (1994).
- [6] G. Tayeb, D. Maystre, J. Opt. Soc. Am. A **14**, 3323 (1997).
- [7] D. Felbacq, G. Tayeb, D. Maystre, J. Opt. Soc. Am. A **11**, 2526 (1994).
- [8] Lie-Ming Li and Zhao-Qing Zhang, Phys. Rev. B **58**, 9587 (1998).
- [9] P. Sabouroux, G. Tayeb, D. Maystre, Opt. Com. **160**, 33 (1999).
- [10] T.A. Birks, J.C. Knight and P.St. J. Russel, Opt. Lett. **22**, 961 (1997).
- [11] S. E. Barkou, J. Broeng and A. Bjarklev, Opt. Lett. **24**, 46 (1998).
- [12] F. Brechet, J. Marcou, D. Pagnoux and P. Roy, Optical Fiber Technology **6**, 181 (2000).
- [13] A. Ferrando, E. Silvestre, J. J. Miret and P. Andrés, Opt. Lett. **25**, 1328 (2000).
- [14] Private communication with F. Zolla.
- [15] F. Zolla, R. Petit, M. Cadilhac, J. Opt. Soc. Am. A. **11**, 1087 (1994).
- [16] P. Vincent, R. Petit, Opt. Com. **5**, 261 (1972).
- [17] Abramowitz and Stegun, *Handbook of mathematical functions*. (Dover, New York,1970).
- [18] D. Felbacq, J. Phys. A **33**, 7137 (2000)
- [19] E. Centeno, D. Felbacq, J. Opt. Soc. Am. A **16**, 2705 (1999).
- [20] A. L. Reynolds, H. Chong, I. G. Thayne, P. J. I. de Maagt and J. M. Arnold, Synthetic Metals, **116** 433 (2001).
- [21] D. Felbacq, E. Centeno, F. Zolla, *Electromagnetic Optics of Finite-size Photonic Crystals: Homogenization, Resonances, Non-linearity and Propagation* to be published in Recent Research Developments in Optics, (Research SignPost Ed., 2001).

Figures captions:

Figure 1: Scattering by a set of parallel fibers of arbitrary shape, optical index and position.

Figure 2: Definition of the incident angle φ_0 , polarization angle δ_0 , conicity angle θ_0 in the Cartesian system (O, x, y, z) .

Figure 3: Hexagonal PC constituted by 19 air hole embedded in a dielectric circular cylinder of optical index $\sqrt{\varepsilon_r} = 4$. When central air hole (dashed fiber) is removed the PC is doped by a microcavity. The radii of the air hole and the cylinder sheath are respectively $r_f = 0.8$ and $R = 10$. The segment below the structure is used for the computation of the transmission coefficient T .

Figure 4: Relative error of the transmission coefficient T versus n_f and n_c . The structure is illuminated by a plane wave in p -polarization and for $\lambda/R = 1.70$.

Figure 5: Diagram of transmission for the PC defined in fig.3 but without the circular cylinder sheath. The hexagonal PC presents a photonic band gap approximately equal to $[2.15; 2.70]$ for p -polarization (bold curve). The solid, dashed and dotted-dashed curves are respectively obtained for the incident field parameters: $\theta_0 = [90^\circ; 80^\circ; 70^\circ]$ and for the same polarization angle $\delta_0 = 0^\circ$.

Figure 6: Logarithm of transmission versus the wavelength for the structure defined in fig.3 and for p -polarization: the solid curve is obtained when the PC is doped by a central microcavity whereas the dashed curve is computed for the perfect PC.

Figure 7: Map of the modulus of the magnetic field for the wavelength associated to the localized mode $\lambda_r^c(90^\circ)/R = 2.20$.

Figure 8: Diagram of transmission for the structure of fig.3 for 3 conicity angles $\theta_0 = [90^\circ; 80^\circ; 70^\circ]$ and for a fixed polarization angle $\delta_0 = 0^\circ$.

Table caption:

Table 1: Comparison between the resonant wavelength versus the conicity angle calculated with a direct numerical computation and thanks equation (9).

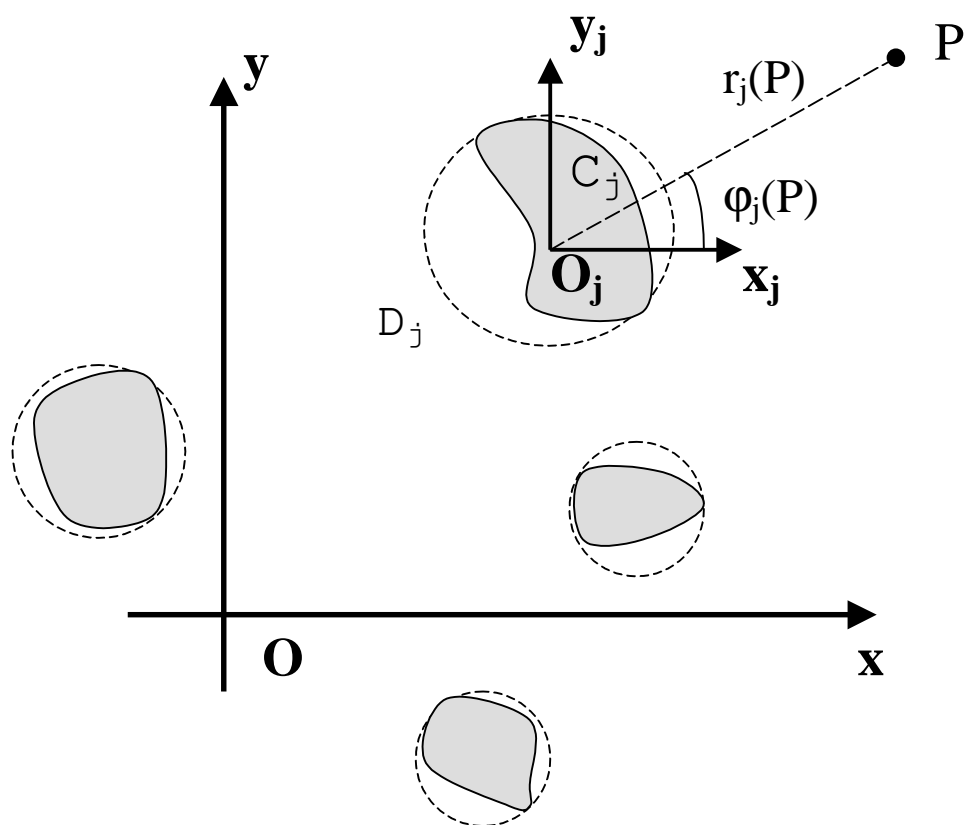
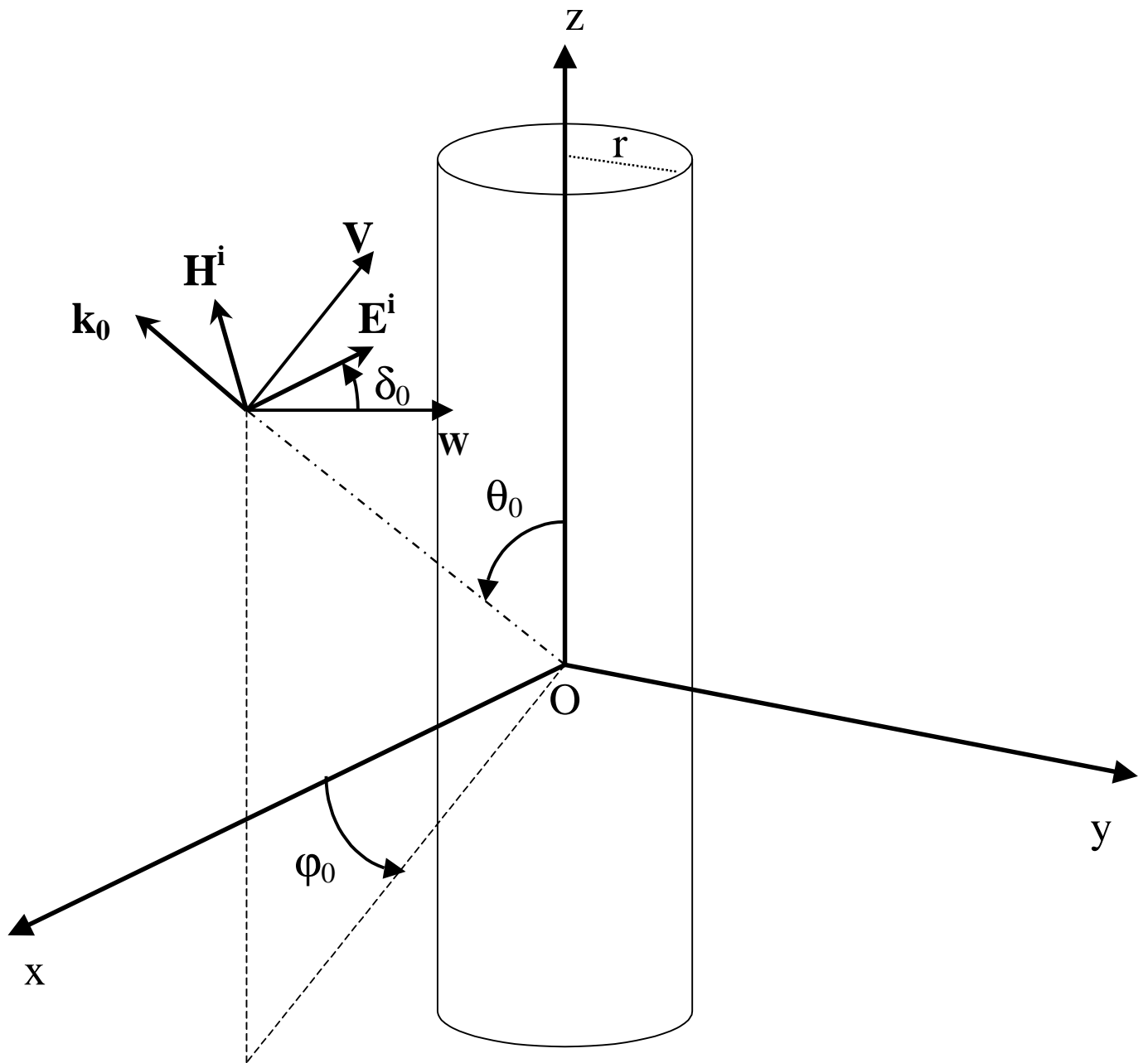


Figure 1

Conicity angle θ_0	Resonant wavelength numerically computed	Resonant wavelength computated thanks eq.(9)
90°	2.12	2.12
80°	2.09	2.088
70°	1.98	1.992

Table 1



$$\mathbf{V} = \sin(\theta_0)\mathbf{e}_z - \cos(\theta_0) \cdot (\cos(\varphi_0)\mathbf{e}_x + \sin(\varphi_0)\mathbf{e}_y)$$

$$\mathbf{W} = -\sin(\varphi_0)\mathbf{e}_x + \cos(\varphi_0)\mathbf{e}_y$$

Figure 2

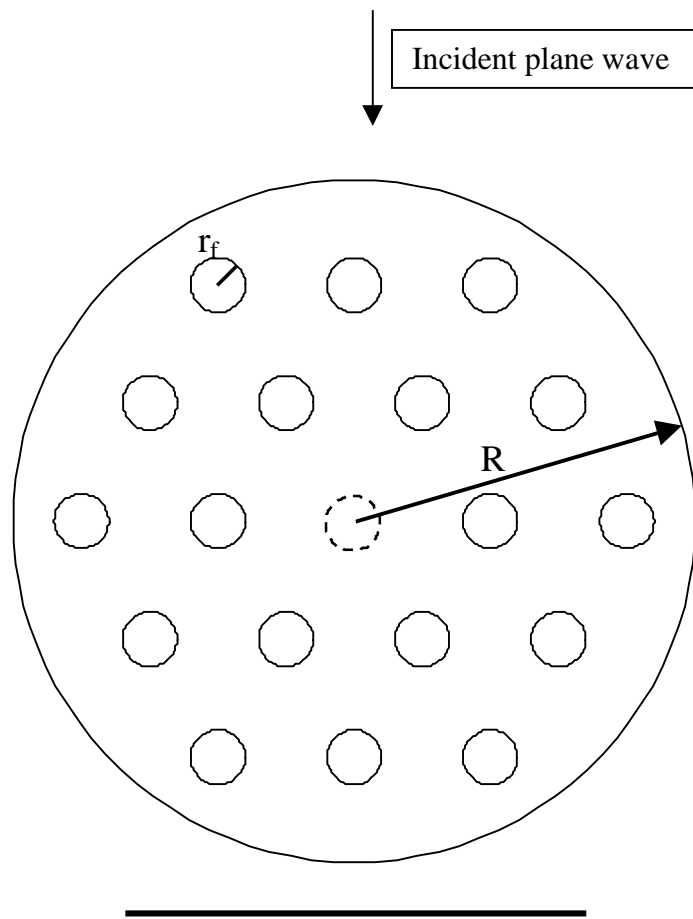


Figure 3

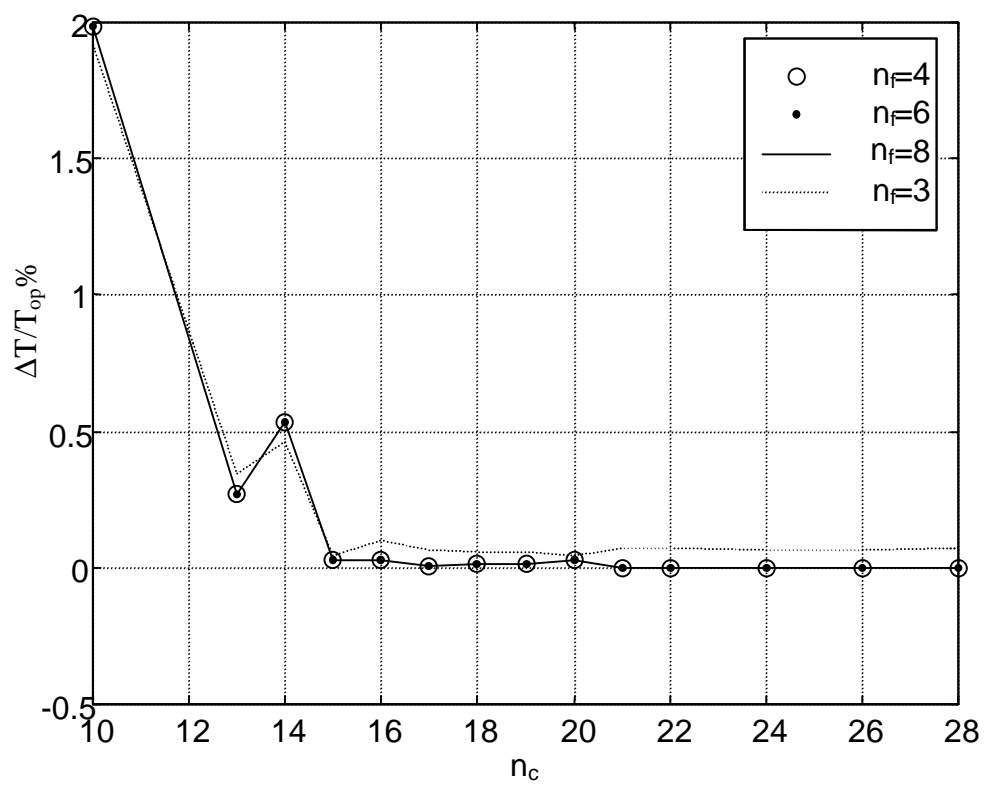


Figure 4

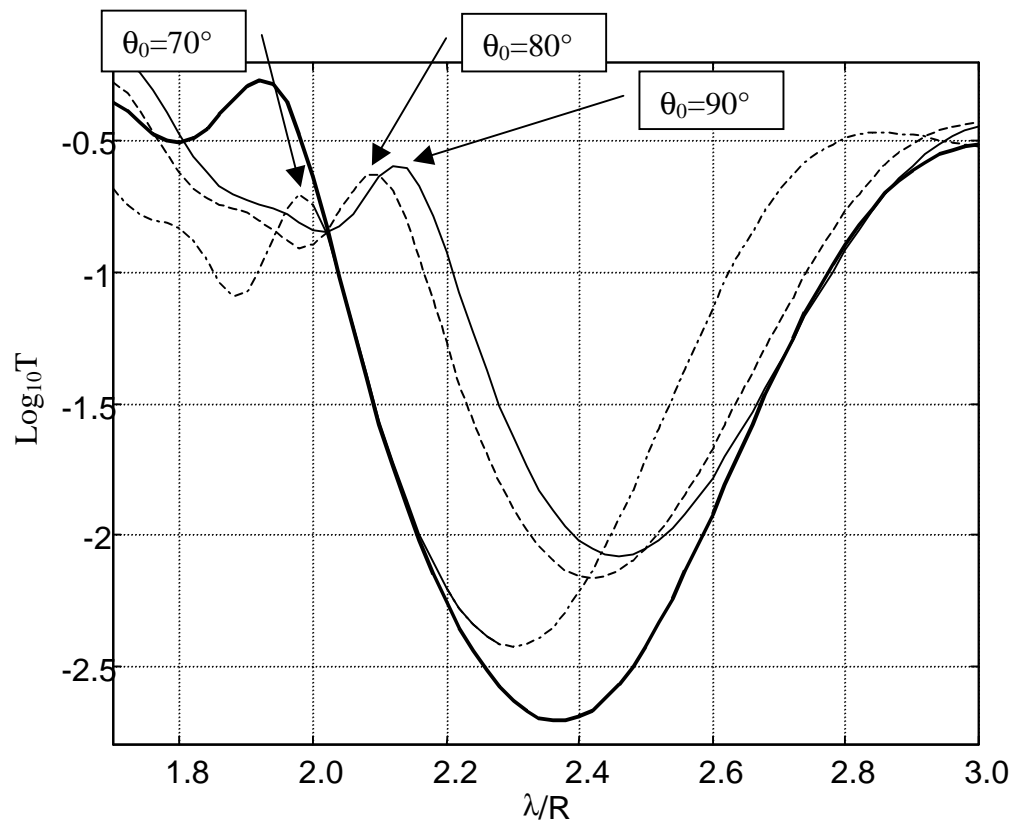


Figure 5

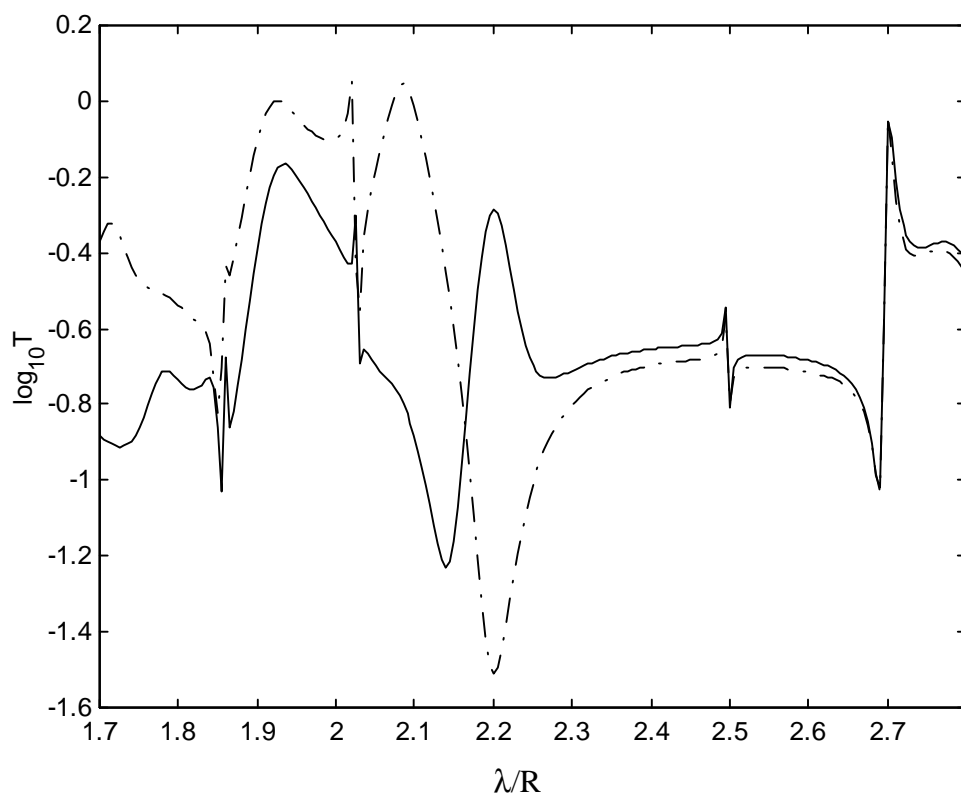


Figure 6

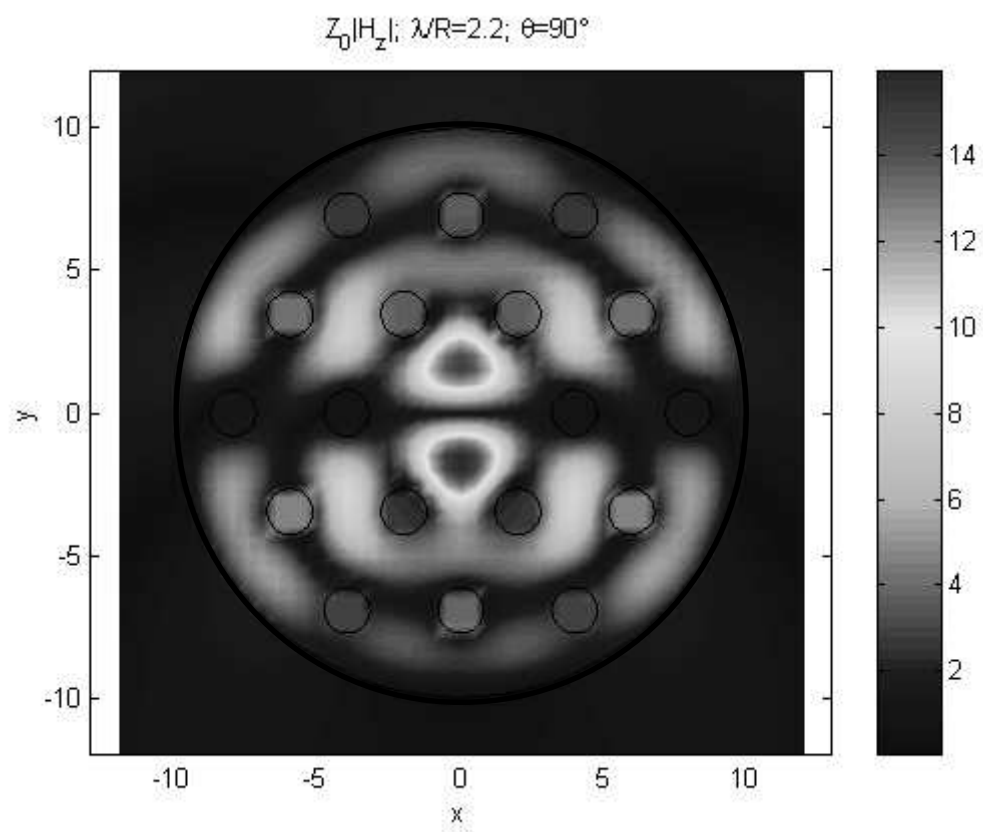


Figure 7

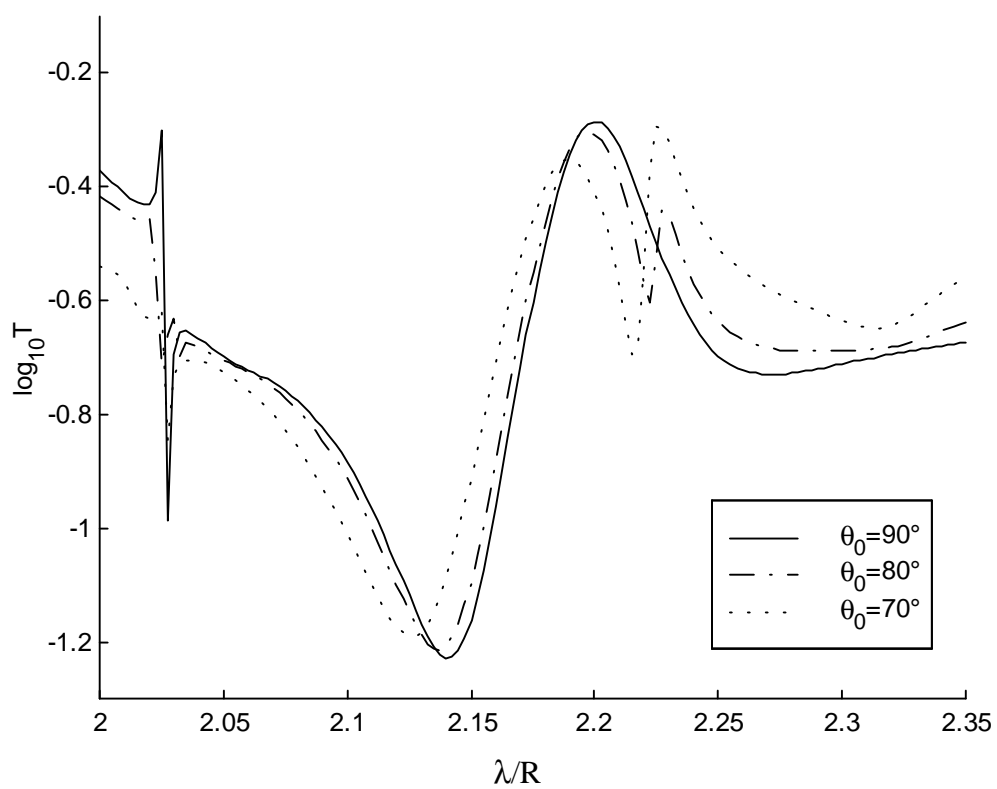


Figure 8